Journal of Integrative Agriculture 2026, 25(3): 879–892

Available online at ScienceDirect

Journal of Integrative Agriculture



RESEARCH ARTICLE

A single nucleotide substitution in *BnaC02.LBD6* promoter causes blade shape variation in *Brassica napus*

Jinxiang Gao[1], Bing Li[2], Pei Qin[3], Sihao Zhang[1], Xiaoting Li[1], Yebitao Yang[1], Wenhao Shen[1], Shan Tang[1], Jijun Li[1], Liang Guo[1, 4], Jun Zou[1], Jinxing Tu[1#]

[1] *National Key Laboratory of Crop Genetic Improvement/College of Plant Science & Technology, Huazhong Agricultural University, Wuhan 430070, China*
[2] *Crop Research Institute, Sichuan Academy of Agricultural Sciences/Sichuan Key Laboratory of Green Germplasm Innovation and Genetic Improvement of Grain and Oil Crops, Chengdu 610066, China*
[3] *College of Agronomy and Biotechnology, Yunnan Agricultural University, Kunming 650201, China*
[4] *Yazhouwan National Laboratory, Sanya 572025, China*

Highlights

- A dominant mutant *INSIDE-ROLLING LEAF1* (*IRL1*) in rapeseed exhibits pleiotropic phenotypes including inward leaf rolling, drooping siliques, semi-dwarfism, and reduced branching.
- *IRL1* encodes *BnaC02.LBD6*, whose elevated expression due to a promoter SNP drives the mutant phenotypes, revealing a novel regulatory mechanism for leaf rolling.
- The rare allele of *BnaC02.LBD6* and its associated transcriptional networks provide valuable genetic resources for ideotype-based breeding in rapeseed.

Abstract

Leaf morphology constitutes a key component of the ideotype, and optimal leaf rolling contributes to compact plant architecture. Rapeseed (*Brassica napus*) is an important oilseed crop; however, the genetic mechanisms underlying leaf shape development remain poorly understood, and corresponding germplasm resources for genetic improvement are limited. In this study, we identified a dominant mutant, *INSIDE-ROLLING LEAF1* (*IRL1*), which exhibits inward leaf rolling due to defective mesophyll cell development. The mutant also displays drooping siliques and a semi-dwarf phenotype, accompanied by a reduction of one to two effective branches. Through map-based cloning and functional complementation assays, we confirmed *BnaC02G0201100ZS* as the causal gene *IRL1*. This gene encodes *LATERAL ORGAN BOUNDARIES DOMAIN6* (*BnaC02.LBD6*). The phenotypic alterations in the *IRL1* mutant result from elevated expression of *BnaC02.LBD6*, driven by a single nucleotide substitution within a DNA binding site in its promoter region. Overexpression of *BnaC02.LBD6* recapitulated the *IRL1* mutant phenotype, confirming its functional role. Haplotype analysis revealed a rare allelic variant in the *BnaC02.LBD6* promoter associated with the unique leaf morphology of *IRL1*. Transcriptomic profiling indicated significant differential expression of genes involved in adaxial–abaxial leaf polarity establishment, secondary metabolic pathways, and hormone signaling networks. Our findings provide novel insights into the genetic regulation of leaf morphogenesis in rapeseed and offer valuable genetic resources for optimizing plant architecture in breeding programs.

Keywords: *Brassica napus*, *LATERAL ORGAN BOUNDARIES DOMAIN* (*LBD*), *BnaC02.LBD6*, leaf shape, map-based cloning, plant architecture

1. Introduction

Leaves serve as the primary source organs for dry matter accumulation in most plants by converting carbon dioxide and water into carbohydrates and oxygen through photosynthesis. To optimize this process, plants precisely regulate leaf initiation, shape, and polarity (Moon and Hake 2011; Du *et al.* 2018). Leaf morphology significantly influences crop yield, and controlled leaf curling can balance maximal light energy

Received 18 February 2024; Received in revised form 7 April 2024; Accepted 6 May 2024; Available online 27 June 2024
Jinxiang Gao, E-mail: gaojx@yaas.org.cn; #Correspondence Jinxing Tu, E-mail: tujx@mail.hzau.edu.cn

© 2026 CAAS. Publishing services by Elsevier B.V. on behalf of KeAi Communications Co. Ltd. This is an open access article under the CC BY-NC-ND license (http://creativecommons.org/licenses/by-nc-nd/4.0/). Peer review under responsibility of Editorial Board of *Journal of Integrative Agriculture*.
doi: 10.1016/j.jia.2024.06.009

capture with reduced transpiration (Govaerts *et al.* 1996; Fang *et al.* 2021). Leaf rolling enhances air circulation and light penetration within plant canopies, lowers the incidence of diseases and pests, and supports high-density planting (Xu *et al.* 2018; Sun *et al.* 2020). Therefore, identifying genes associated with leaf rolling and elucidating their molecular mechanisms hold practical importance for crop breeding programs.

Leaf shape is determined by three developmental axes: proximal–distal, medio–lateral, and abaxial–adaxial (Canales *et al.* 2005; Dkhar and Pareek 2014; Satterlee and Scanlon 2019). These axes are coordinately regulated by transcription factors, microRNAs (miRNAs), and hormonal signaling pathways (Xu *et al.* 2018; Wang *et al.* 2021). The abaxial–adaxial axis plays a central role in determining leaf rolling, and substantial progress has been made in characterizing the regulatory networks governing leaf morphogenesis.

Three class III homeodomain-leucine zipper (HD-ZIP III) transcription factors — REVOLUTA, PHABULOSA, and PHAVOLUTA — are critical for adaxial cell fate specification (McConnell and Barton 1998; McConnell *et al.* 2001; Emery *et al.* 2003). Mutations in HD-ZIP III genes often result in disrupted polarity and leaf curling (Itoh *et al.* 2008; Rong *et al.* 2019). miRNA165 and miRNA166 negatively regulate HD-ZIP III gene expression, thereby influencing adaxial development (Prigge *et al.* 2005; Chitwood *et al.* 2007; Tatematsu *et al.* 2015). ASYMMETRIC LEAVES1 (AS1), an MYB domain-containing transcription factor, forms a repressor complex with ASYMMETRIC LEAVES2 (AS2), a LATERAL ORGAN BOUNDARIES domain protein. This AS1/AS2 complex positively regulates HD-ZIP III genes to promote adaxial identity (Husbands *et al.* 2015; Merelo *et al.* 2016). In contrast, the abaxial side is primarily governed by members of the KANADI (KAN) family, the YABBY (YAB) family, and AUXIN RESPONSE FACTORs (ARFs).

KAN proteins contain a GARP DNA-binding domain, and both loss-of-function mutations and overexpression of KAN genes lead to defects in leaf polarity (Eshed *et al.* 2001; Kerstetter *et al.* 2001; Eshed *et al.* 2004). KAN1 antagonizes the AS1/AS2 complex and HD-ZIP III activity, ensuring proper establishment and maintenance of adaxial–abaxial polarity (Wu *et al.* 2008; Chen *et al.* 2013; Caggiano *et al.* 2017; Merelo *et al.* 2017; Manuela and Xu 2020). ARF2, ARF3, and ARF4 are expressed on the abaxial side of leaves, where they promote abaxial cell differentiation. These ARFs act as suppressors in KAN-overexpressing plants, and their mutant phenotypes resemble those of KAN loss-of-function mutants (Pekker 2005; Kelley *et al.* 2012; Guan *et al.* 2017). The YAB family contributes to abaxial development (Siegfried *et al.* 1999; Bowman 2000; Romanova *et al.* 2021) and is positively regulated by both KANs and ARFs (Eshed *et al.* 2004; Garcia *et al.* 2006). Simultaneous mutations in the functionally redundant genes YAB1, YAB2, and YAB3 disrupt adaxial–abaxial polarity, leading to severe developmental defects (Stahle *et al.* 2009; Sarojam *et al.* 2010).

Rolling leaf germplasm has been utilized in the genetic improvement of major crops such as rice, wheat, and maize (Pan *et al.* 2020; Fang *et al.* 2021; Yu *et al.* 2022; Zhu *et al.* 2022; Wang *et al.* 2023). Rapeseed, a globally significant oilseed crop, remains underexplored in terms of leaf curling-related genes, and limited germplasm resources are available for modifying its leaf architecture.

In this study, we identified a novel rapeseed mutant, *INSIDE-ROLLING LEAF1* (*IRL1*). Using map-based cloning and genetic complementation, we confirmed that *BnaC02.LBD6* is the causal gene. We further demonstrated that *BnaC02.LBD6* is homologous to *Arabidopsis* AS2; a single nucleotide substitution in its promoter region leads to elevated expression in the *IRL1* mutant; the *IRL1* mutant exhibits pleiotropic traits including reduced plant height, drooping siliques, and fewer effective branches; and the heterozygous genotype displays an ideal plant architecture due to single-locus dominance. These findings underscore the critical role of *BnaC02.LBD6* in shaping rapeseed plant architecture and highlight its potential utility in breeding improved rapeseed varieties.

2. Materials and methods

2.1. Plant materials and growth conditions

The *IRL1* mutant was identified from an ethyl methane sulfonate (EMS) mutagenized library of ZS11, a Chinese open-pollinated cultivar (Tang *et al.* 2020), and crossed with Westar to generate F_1, F_2, and BC_1 populations for genetic analysis and fine mapping. To evaluate yield traits, ZS11 was hybridized with the inbred line 7112. The mapping population was grown in Wuhan, Hubei Province, China (29°58′N, 113°41′E) in October and in Lanzhou, Gansu Province, China (36°03′N, 103°40′E) in May each year, with row spacing of 15 and 10 cm, respectively, and 10–15 plants per row. Yield-related traits were assessed under field conditions. *Arabidopsis* and tobacco were cultivated in a greenhouse under a 16-h light/8-h dark photoperiod at a constant temperature of 20°C.

2.2. Paraffin section

Paraffin sections were prepared to examine mesophyll cell development. The penultimate true leaf at the five-leaf stage was collected, fixed in 50% FAA (formalin-acetic acid-alcohol) solution, subjected to vacuum infiltration for 30 min, and sectioned following a previously described protocol (Li *et al.* 2023). Observations were recorded using a microscope (Nikon, Tokyo, Japan), and images were captured for subsequent statistical analysis with ImageJ.

2.3. Map-based cloning

A mapping population was developed by crossing the *IRL1* mutant with the divergent variety Westar. Bulked segregant analysis was performed using DNA pools from F_2 individuals: two pools each for rolling- and normal-leaf phenotypes (10 plants per pool), along with separate pools for the *IRL1* mutant and Westar parents. The *Brassica* 50K SNP Bead Chip Array was employed for initial mapping according to established methods (Li *et al.* 2023). Simple sequence repeat (SSR) markers were designed using WebSat (https://bioinfo.inf.ufg.br/websat/), while intronic polymorphism (IP) markers were manually designed within intron regions. These markers were screened for polymorphisms using the

six DNA pools. Polymorphic markers were subsequently used to identify recombination events for fine mapping.

2.4. Construction of transgenic plants

The mutated gene *BnaC02.lbd6* was amplified, including a 2,022-bp putative promoter region and a 738-bp downstream sequence. This fragment was cloned into the pCMBIA2300 vector and introduced into Westar *via* hypocotyl dipping (Dun *et al.* 2011). For *Arabidopsis* transformation, the floral dip method was used (Clough and Bent 1998). Additionally, the CDS of *BnaC02.LBD6* was amplified from ZS11 cDNA, inserted into the overexpression vector pCMBIA2306, and transformed into both Westar and *Arabidopsis.*

2.5. Histochemical β-glucuronidase (GUS) staining

The putative promoter region of *BnaC02.LBD6* was cloned from both the *IRL1* mutant and wild-type (WT) ZS11, ligated into the pCMBIA2300-GUS vector, and transformed into *Arabidopsis*. Tissues from various developmental stages of T_2 transgenic lines were collected and subjected to GUS staining. Stained samples were visualized and imaged using a microscope, following a published protocol (Li *et al.* 2019).

2.6. Subcellular localization

The coding sequences (CDS) of *BnaC02.LBD6* lacking the stop codon was amplified from leaf cDNA of ZS11 and fused in-frame with the green fluorescent protein (GFP) coding sequence in the pMDC83 vector under the control of the cauliflower mosaic virus 35S promoter (35S: *BnaC02.LBD6*-GFP). The construct, along with the nuclear marker H2B-mCherry, was transformed into *Agrobacterium* strain GV3101. H2B-mCherry serves as a nuclear localization control (Howe *et al.* 2012).

Leaves of 4-wk-old tobacco plants were infiltrated with a bacterial suspension of GV3101 carrying *BnaC02.LBD6*-GFP and H2B-mCherry. Subcellular localization was examined 3 days post-infiltration using a confocal laser scanning microscope (SP2; Leica Microsystems, Wetzlar, Germany).

2.7. Yeast one-hybrid assay (Y1H)

KAN1 directly binds to the AS2 promoter to regulate its activity (Wu *et al.* 2008). Among homologs, *BnaA03.KAN1* (*BnaA03G0070500ZS*) exhibits the highest sequence similarity to AtKAN1 and is highly expressed in leaves, making it a suitable candidate for Y1H analysis. The full-length CDS of *BnaA03.KAN1* was amplified and cloned into the pB42AD vector (Clontech, USA), generating the AD-KAN1 plasmid. Normal and single-nucleotide-substituted versions of the AS2 promoter sequence were synthesized and cloned into the LacZ reporter vector (pLacZi2μ). These reporter constructs were co-transformed with either AD-KAN1 or empty pB42AD (negative control) into yeast strain EGY48. Transformants were grown on selective medium containing *X-gal* (*5-bromo-4-chloro-3-indolyl-β-D-galactopyranoside*) at 25°C for approximately 8 h. Yeast transformations were carried out according to the Yeast Protocols Handbook (Clontech).

2.8. RNA extraction and qRT-PCR

Tissues from rapeseed — including roots, stems, leaves, buds, pods, and seeds — as well as *Arabidopsis* leaves, were harvested and immediately frozen in liquid nitrogen. Total RNA was extracted using the Total RNA Isolation Kit (TINAGEN, Beijing, China). First-strand cDNA was synthesized using the RevertAid First Strand cDNA Synthesis Kit (Thermo Fisher Scientific, Waltham, MA, USA). qRT-PCR was conducted on a CFX96 Touch Real-Time PCR Detection System (Bio-Rad Laboratories, Hercules, CA, USA) with SYBR Green Supermix (Toyobo, Japan). *BnActin7* (*BnaA03G0037300ZS*) served as the reference gene in rapeseed, and *AtActin2* (*AT3G18780*) in *Arabidopsis*. Relative gene expression levels were calculated using the method described by Li *et al*. (2019).

2.9. Transcriptome analysis

The first true leaves from 4-leaf-stage seedlings of Westar and transgenic complementation lines (T_3 generation) were collected for RNA-seq with three biological replicates. Tissues were rapidly frozen in liquid nitrogen. A subset of RNA-seq data was validated by qRT-PCR. Total RNA was isolated using Trizol Reagent (Invitrogen, USA). Sequencing was performed on an Illumina NovaSeq 6000 platform by Shanghai Personal Biotechnology Co. (Shanghai, China). Raw reads were processed using fastp to remove low-quality sequences and adapter contaminants (Chen *et al.* 2018). Clean reads were aligned to the *Brassica napus* reference genome (http://cbi.hzau.edu.cn/cgi-bin/rape/download_ext) using TopHat2 (Kim *et al.* 2019). Gene expression levels were quantified as fragments per kilobase million (FPKM) using feature Counts (Liao *et al.* 2014). Differentially expressed genes (DEGs) were identified using DESeq2 with thresholds of $|\log_2(\text{fold change})|>1$ and adjusted *P*-value<0.05 (http://www.bioconductor.org/packages/release/bioc/html/DESeq2.html). Functional annotation, classification, and pathway enrichment analyses were conducted using Gene Ontology (GO, http://www.geneontology.org) and Kyoto Encyclopedia of Genes and Genomes (KEGG) (https://www.kegg.jp/) databases.

2.10. Haplotype analysis

Leaf area was used as a phenotypic indicator of natural variation. Phenotypic data were obtained from two natural populations comprising 991 and 505 accessions (Wu *et al.* 2019; Tang *et al.* 2021). Genotypic data were downloaded from the *B. napus* Multi-Omics Database (https://yanglab.hzau.edu.cn/BnIR). The genomic region encompassing LBD6 and its flanking ±1.5 kb sequences was selected for haplotype analysis.

2.11. Cleaved amplified polymorphic sequence marker (CAPS) development

Primers CAPS-LBD6-F and CAPS-LBD6-R were designed to amplify a 400-bp fragment spanning the mutation site. The SNP was centered, with 29 bp extended upstream and downstream. The dCAPS primer dCAPS-LBD6-R2 was designed using dCAPS Finder 2.0 (http://helix.wustl.edu/

dcaps/dcaps.html), incorporating the restriction enzyme *Bsa*BI (recognition site: GATNNNNATC), and paired with CAPS-LBD6-F. A 200-bp product derived from the 400-bp amplicon was digested with Thermo Scientific Fast Digest enzyme and analyzed *via* polyacrylamide gel electrophoresis. The *IRL1* mutant contains a single nucleotide substitution that abolishes the BsaBI recognition site, preventing digestion.

2.12. Statistical analysis

All quantitative data were analyzed using GraphPad Prism 8. Statistical significance was determined by Student's *t*-test: *, $P<0.05$; **, $P<0.01$; ***, $P<0.001$. For multiple comparisons, ANOVA followed by Bonferroni's *post-hoc* test was applied, with different letters indicating significant differences at $P<0.05$.

3. Results

3.1. *IRL1* mutant exhibits leaf rolling, drooping siliques, semi-dwarf stature, and decreases in effective branches

The IRL1 mutant was identified from the EMS-mutagenized library of ZS11 (ZS11, a Chinese open-pollination cultivar, wild type (WT)). Leaves of the *IRL1* mutant exhibited upward curling along the main vein, maintaining an upright, rolled conformation throughout development, whereas WT leaves were nearly flat and symmetrical (Fig. 1-A–C), resulting in significant differences in leaf width between genotypes (Fig. 1-E). During flowering, in contrast to the upward-growing buds and siliques in WT plants, the *IRL1* mutant displayed drooping buds and siliques, with a significantly altered silique angle (Fig. 1-D–F). At maturity, the *IRL1* mutant showed a semi-dwarf phenotype, with a plant height of (90±3.6) cm, approximately 50% of that of WT ((181±5.4) cm; Fig. 1-C and F). Additionally, the number of effective branches was significantly reduced in *IRL1*, and F_1 hybrids (with ZS11 as the maternal parent and *IRL1* as the paternal parent) exhibited one or two fewer effective branches than WT (Fig. 1-C and E). Due to the upright and rolled leaf architecture of *IRL1*, individual plants occupied less space, conferring tolerance to dense planting in the hybrid F_1 (Appendix A). Yield trait analysis revealed that thousand-seed weight remained unchanged in both *IRL1* and F_1 compared to WT, but seed yield per plant decreased by approximately 40% in *IRL1* and by only 14% in F_1 (Appendix B). Collectively, these findings demonstrate that *IRL1* exerts pleiotropic effects on rapeseed growth and development.

3.2. Abnormal mesophyll cell development in the *IRL1* mutant

To investigate the cellular basis of leaf rolling in the *IRL1* mutant, paraffin sections of the penultimate true leaf at the five-leaf stage were examined (Fig. 2-A). No differences were observed in vascular tissue development at the petiole level (Fig. 2-B), indicating that leaf morphology changes are not attributable to vascular defects. Instead, pronounced differences were evident in mesophyll cell structure. In WT, cells surrounding the leaf vein vascular bundles were large with minimal intercellular spaces; in contrast, *IRL1* mesophyll cells were smaller and exhibited enlarged intercellular spaces (Fig. 2-C). Furthermore, the palisade mesophyll in *IRL1* consisted of a single layer of small, loosely arranged cells, whereas WT possessed at least two layers of large, tightly packed palisade cells (Fig. 2-D–F). Although sponge mesophyll area did not differ significantly, WT spongy parenchyma cells were densely packed with narrow intercellular spaces, while those in *IRL1* were loosely organized with expanded gaps (Fig. 2-D, G, and H). These observations indicate that abnormal mesophyll cell development underlies the altered leaf morphology in the *IRL1* mutant.

3.3. Map-based cloning identifies the causal gene *IRL1*

To determine the genetic inheritance pattern, reciprocal crosses were performed between the *IRL1* mutant and WT. The F_1 progeny exhibited phenotypes resembling the *IRL1* mutant, including rolled leaves, reduced stature, and drooping buds and siliques (Fig. 1-A, C, and D), suggesting dominant inheritance of *IRL1*. Phenotypic segregation analysis in F_2 and BC_1 populations revealed ratios of rolled-to-normal leaves of 3:1 and 1:1, respectively (Fig. 3-A), consistent with a single dominant mutation. This inheritance pattern was further confirmed in a segregating population derived from crossing *IRL1* with Westar, a Canadian cultivar with a distinct genetic background, which was used for mapping.

Bulked segregant analysis combined with the *Brassica* 50 K SNP Bead Chip Array was employed to locate the causal gene. A total of 112 polymorphic SNPs were identified, with 56 clustered on chromosome C02 (ChrC02), 16 on ChrC01, and the remainder dispersed across other chromosomes (Fig. 3-B; Appendix C). SSR markers within regions covered by differential SNPs on Clustered on ChrC02 and ChrC01 were screened, and polymorphisms were detected only on ChrC02, indicating the gene's chromosomal location. Using 561 normal-leaf individuals from F_2 and BC_1 populations, recombination events were analyzed, narrowing the candidate region to a ~1.8 Mb interval flanked by markers L71 and N24 (Fig. 3-C). Subsequently, additional SSR and IP markers were developed within this region, and fine mapping using 7,828 normal-leaf F_2 individuals delimited the causal gene to a ~128 kb segment between markers IP3-2 and IP2-25, co-segregating with IP2-4 (Fig. 3-D). Annotation of this region based on the ZS11 reference genome (https://yanglab.hzau.edu.cn/BnIR) revealed five predicted genes (Fig. 3-E). DNA sequencing of these candidates — including 2 kb upstream and 1 kb downstream — identified a single nucleotide substitution exclusively in the promoter of *BnaC02G0201100ZS*, with no variation in the other four genes (Fig. 3-F; Appendix D). *BnaC02G0201100ZS* encodes *LATERAL ORGAN BOUNDARIES DOMAIN6* (*BnaC02.LBD6*), a member of the LOB family characterized by a conserved C-x(2)-C-x(6)-C-x(3)-C motif (Appendix E). *BnaC02.LBD6* shares 75.38% protein sequence identity with *Arabidopsis* AS2 (Appendix F), a known regulator of adaxial–abaxial leaf polarity essential for symmetric lamina formation. Previous studies have shown that *as2* mutants exhibit leaf rolling (Wu *et al.* 2008; Chen *et al.* 2013). Together, these

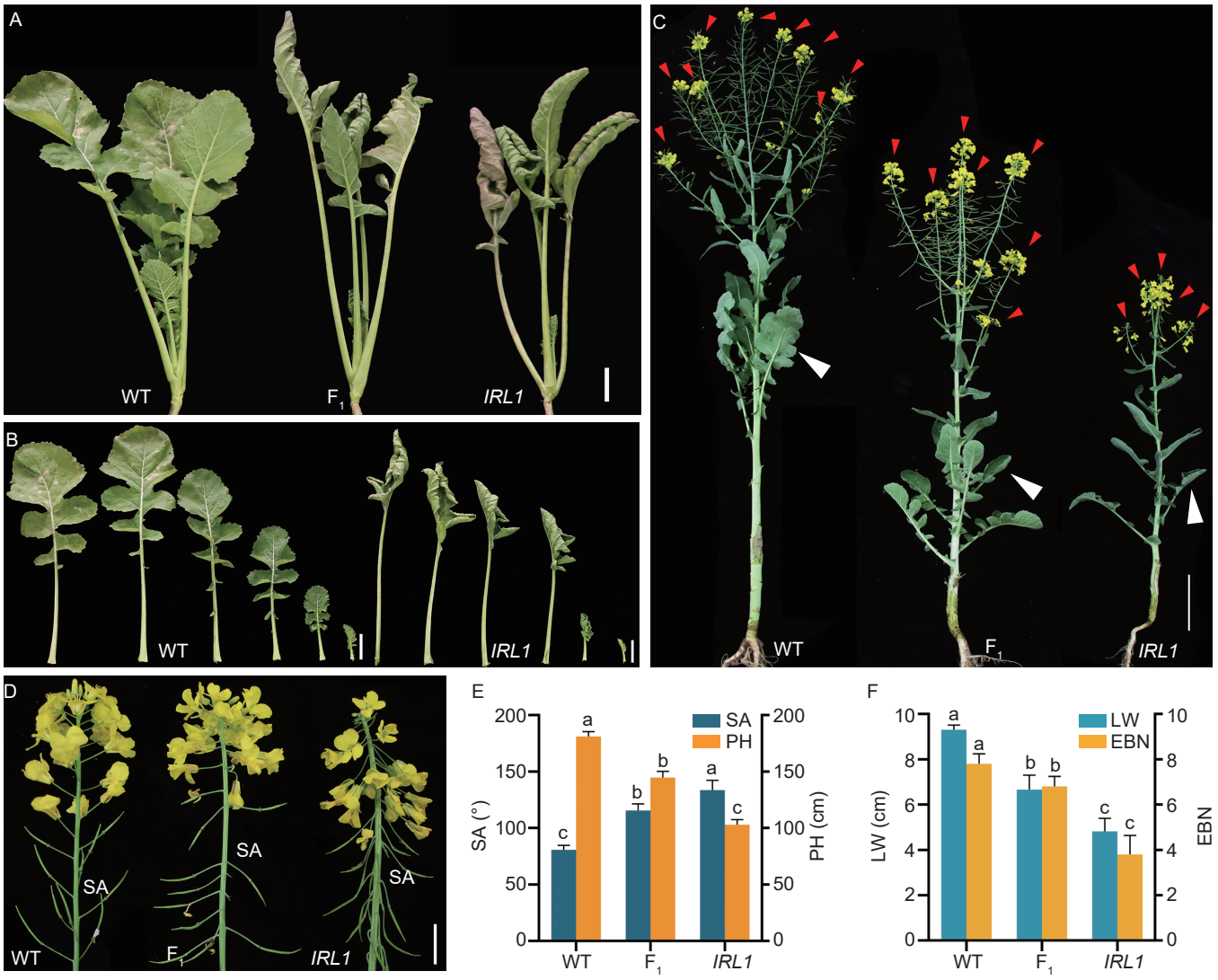


Fig. 1 Phenotypic characterization of the *IRL1* mutant. A, comparison of leaf morphology at the six-leaf stage. Bar=3 cm. B, comparison of leaf morphology at different developmental stages. Bar=3 cm. C, comparison of plant height at the flowering stage. Bar=5 cm. D, comparison of bud and silique phenotypes. The F_1 plants exhibited an intermediate phenotype. Bar=2 cm. E, statistical analysis of silique angle and plant height. LW, leaf width; EBN, effective branch number; SA, silique angle; PH, plant height. F, statistical analysis of leaf width and effective branch number. Bars in E and F mean SD (n=15). Data significance was assessed using Student's t-test: **, P<0.01; ***, P<0.001.

data identify *BnaC02.LBD6* as the candidate causal gene IRL1 located on ChrC02.

3.4. *BnaC02.LBD6* is the causal gene *IRL1*, primarily regulating phenotypic variation through expression level modulation

To test whether the single nucleotide substitution in the *BnaC02.LBD6* promoter is responsible for the *IRL1* phenotype, a transgenic vector containing *BnaC02.LBD6* under its mutated promoter was introduced into Westar (Appendix E). T_0 transgenic plants exhibited a leaf-rolling phenotype similar to *IRL1*, which was stably inherited in the T_1 generation (Fig. 4-A). Transgenic-positive lines also displayed drooping buds and siliques, recapitulating the *IRL1* phenotype. These results confirm that the promoter mutation alone is sufficient to induce the mutant phenotype. Moreover, expression levels of *BnaC02.LBD6* were significantly elevated in complementation lines (Fig. 4-B).

To further validate the role of *BnaC02.LBD6* expression in phenotypic variation, an overexpression construct was generated and transformed into Westar. T_0 plants exhibited leaf rolling, and qRT-PCR confirmed strong upregulation of *BnaC02.LBD6* (Fig. 4-C and D). Both complementation and overexpression constructs were also introduced into *Arabidopsis*. Transgenic *Arabidopsis* lines displayed leaf rolling, drooping buds, and siliques; some exhibited extreme phenotypes, including severely curled leaves, dwarfism, and reduced seed set (Fig. 4-E). Overexpressing lines showed particularly severe developmental defects, such as needle-like leaves and complete failure to flower or set fruit (Fig. 4-F). qRT-PCR analysis revealed a positive correlation between the severity of phenotypic abnormalities and the expression level of *BnaC02.LBD6* (Fig. 4-G and H). These findings

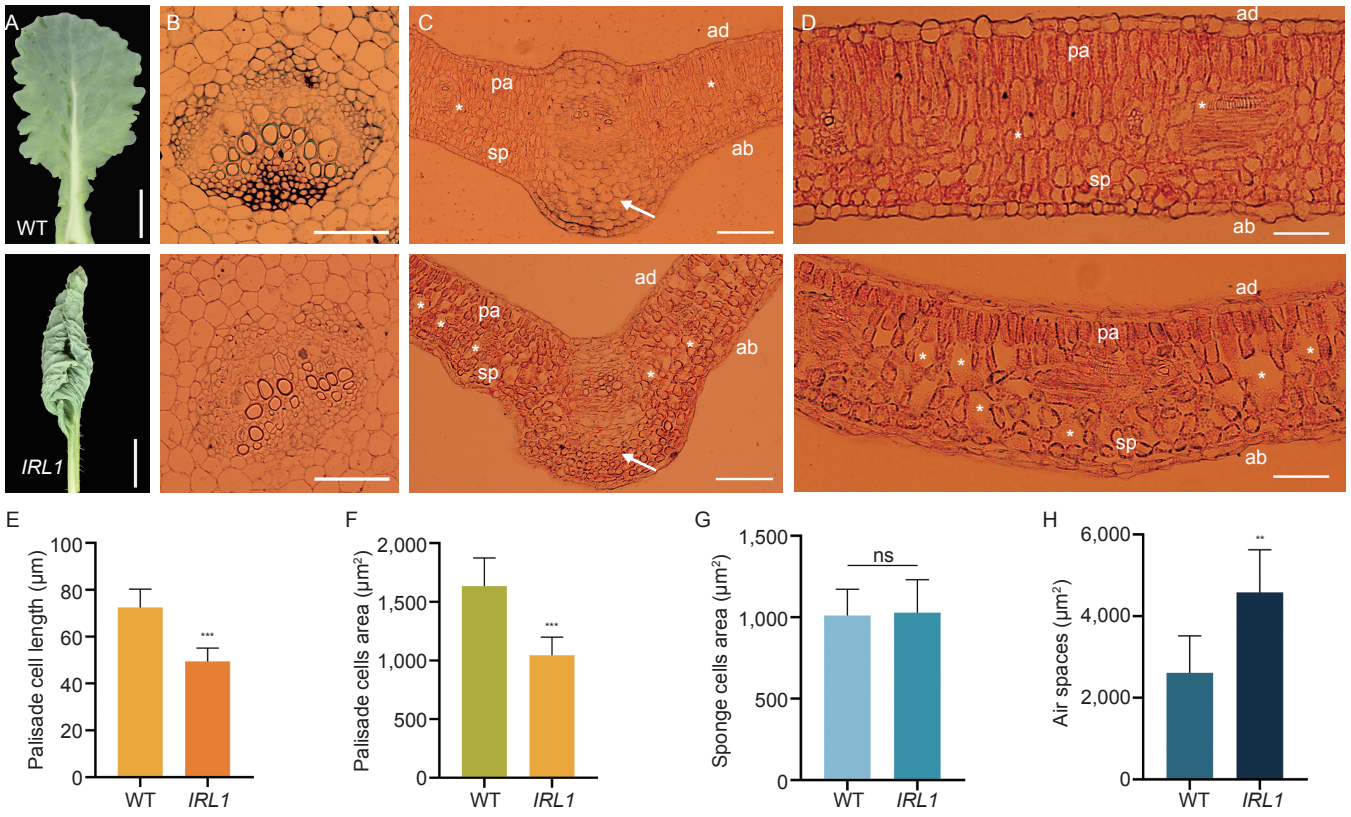


Fig. 2 Leaf phenotypic variation revealed by paraffin sectioning. A, leaf sample used for paraffin sectioning. Bar=1 cm. B, no observable differences in vascular tissue development at the petiole. Bar=100 μm. C, abnormal peripheral cell development within vascular bundles of leaf veins. Bar=100 μm. pa, palisade mesophyll cells; sp, spongy mesophyll cells; asterisks indicate air spaces; ad and ab denote the adaxial and abaxial sides of the leaf, respectively. D, disrupted development of mesophyll cells. Bar=100 μm. E–H, statistical analyses of palisade cell length, palisade cells area, sponge cells area, and air spaces. Bars in E–H mean SD (n=15). Data significance was assessed using Student's t-test: **, P<0.01; ***, P<0.001; ns, not significant.

demonstrate that the *IRL1* phenotype arises from a single nucleotide substitution in the *BnaC02.LBD6* promoter that increases its expression, and the extent of phenotypic alteration is dosage-dependent.

3.5. *BnaC02.LBD6* is predominantly expressed in leaves and buds, and the protein localizes to the nucleus

To characterize the expression pattern of *BnaC02.LBD6*, qRT-PCR was performed using total RNA isolated from root, stem, leaf, bud, silique, and seed tissues of ZS11. *BnaC02.LBD6* was expressed in all tested tissues, with highest levels in leaves and buds, and lower expression in roots, stems, siliques, and seeds (Fig. 5-A). Comparative analysis in near-isogenic lines revealed no significant differences in expression at the root, leaf apex, or leaf vein; however, higher expression was detected in rolled-leaf lines in stems, leaf margins, petioles, and buds (Fig. 5-B), reinforcing the link between *BnaC02.LBD6* abundance and phenotypic variation (Fig. 4-G and H). To visualize spatial expression, GUS reporter constructs driven by either the WT or mutated *BnaC02.LBD6* promoter were introduced into *Arabidopsis*. GUS staining showed strong signals in leaves, stems, and silique pedicels in lines carrying the mutated promoter (Fig. 5-C), mirroring the leaf rolling and drooping phenotypes of *IRL1*. To determine subcellular localization, the *BnaC02.LBD6* coding sequence was fused to GFP and transiently expressed in tobacco. *BnaC02.LBD6*-GFP fluorescence overlapped with the nuclear marker H2B-mCherry (Fig. 5-D), confirming that *BnaC02.LBD6* is a nuclear-localized protein.

3.6. A single nucleotide substitution in the *BnaC02.LBD6* promoter represents a rare allelic variant

To assess whether natural variation in *BnaC02.LBD6* influences leaf morphology, haplotype analysis was conducted across a diverse panel of over 1,000 *B. napus* accessions, covering the gene and its ±1.5 kb flanking regions. Among 53 identified variants, the SNP present in the *IRL1* mutant promoter was unique and absent in all natural accessions (Appendices G-a and H). Based on these polymorphisms, two major haplotypes were defined: hapC02-0 and hapC02-1 (Appendix I). No significant difference in leaf area was observed between these haplotypes (Appendix G-c). *BnaA02G0157500ZS* (*Brassica napus* Multi-omics Information Resource (https://yanglab.hzau.edu.cn/BnIR) *BnaA02G0157500ZS* (*BnaA02.LBD6*), a homologous copy of *BnaC02.LBD6* available in the *Brassica napus* Multi-omics Information Resource, shares 99.18% DNA sequence identity and exhibits a similar expression profile (Appendix J). Given this high similarity, haplotype

A

Population	Rolling leaf	Normal leaf	Expected ratio	χ^2 value[1)]
F_2-1	367	120	3:1	0.017
F_2-2	399	118	3:1	1.192
BC_1-1	368	350	1:1	0.403
BC_1-2	150	163	1:1	0.626

[1)] $\chi^2_{(0.05,1)}$=3.841.

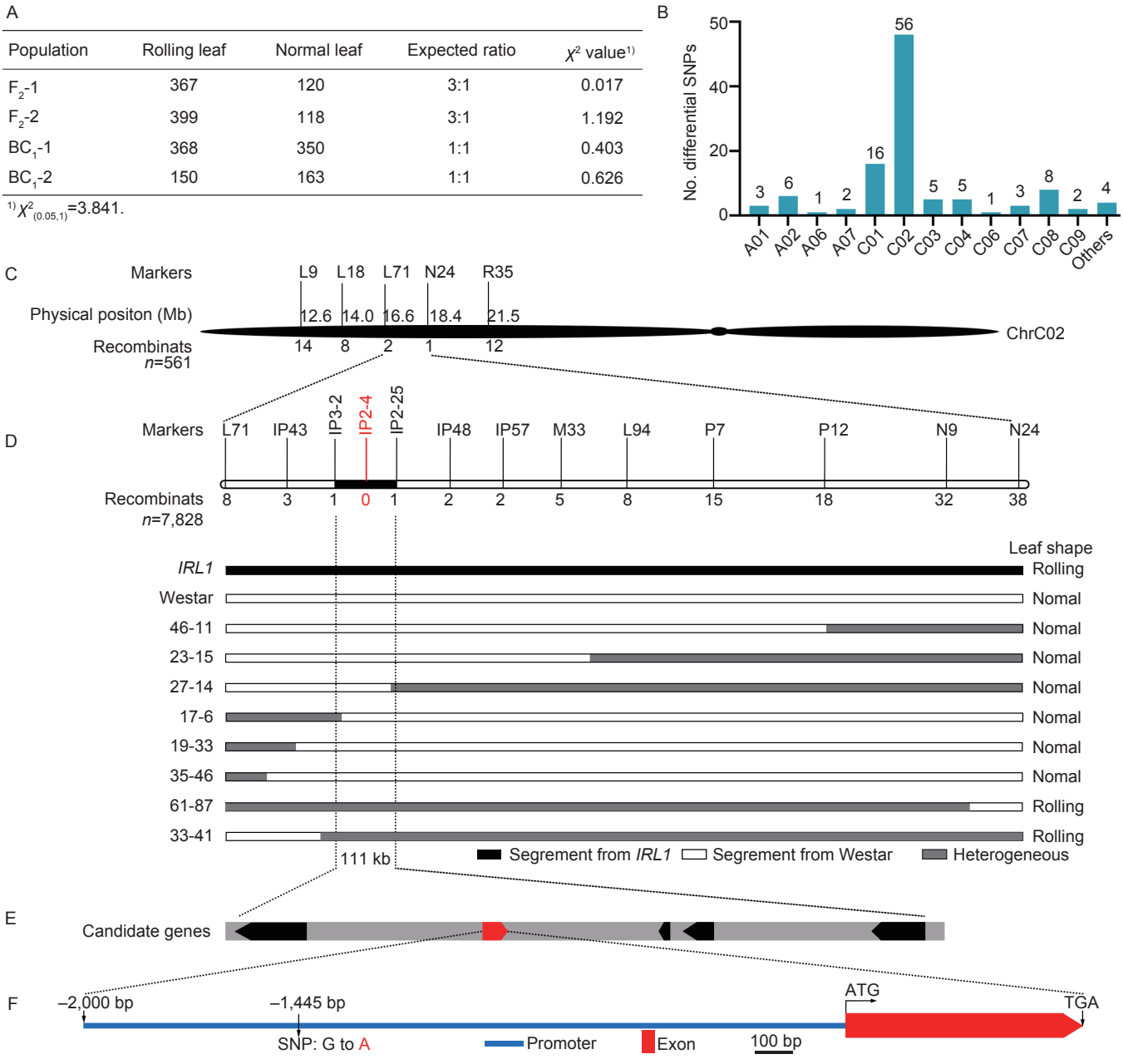


Fig. 3 Map-based cloning of *IRL1*. A, segregation ratio statistics for F_2 and BC_1 populations. B, analysis using the *Brassica* 50 K SNP Bead Chip Array identified 112 polymorphic SNPs. C, preliminary mapping of *IRL1* delimited the locus to a ~1.8 Mb region between markers L71 and N24, based on 561 normal-leaf individuals. D, fine mapping of *IRL1* further narrowed the candidate region to a ~128 kb interval between markers IP3-2 and IP2-25, using 7,828 normal-leaf individuals from the F_2 population. E, genes within the candidate interval; the 128 kb region encompasses five predicted genes. F, DNA sequence variation analysis of candidate genes revealed that *BnaC02G0201100ZS* contains a single exon, and a single nucleotide substitution was detected 1,445 bp upstream of the start codon in the *IRL1* mutant.

analysis was extended to *BnaA02.LBD6* and its flanking regions, revealing 99 variants classified into six haplotypes (hapA02-0 to hapA02-5; Appendices G-b, K, and L). Notably, the position corresponding to the *IRL1* mutation site showed no variation. No differences in leaf area were found among the six *BnaA02.LBD6* haplotypes (Appendix G-d). These results indicate that the single nucleotide substitution in the *BnaC02.LBD6* promoter is a rare, artificial allele not present in natural populations, leading to the unique phenotypic traits observed in the *IRL1* mutant.

3.7. *BnaC02.LBD6* preferentially regulates genes involved in hormone signalling and secondary metabolite processes related genes

To elucidate the molecular mechanisms underlying *BnaC02.LBD6*-mediated developmental regulation, transcriptome profiling was performed on leaf tissues from Westar and transgenic homozygous lines at the four-leaf stage, with three biological replicates. A total of 4,433 differentially expressed genes (DEGs) were identified in the mutant background: 2,762 upregulated and 1,671

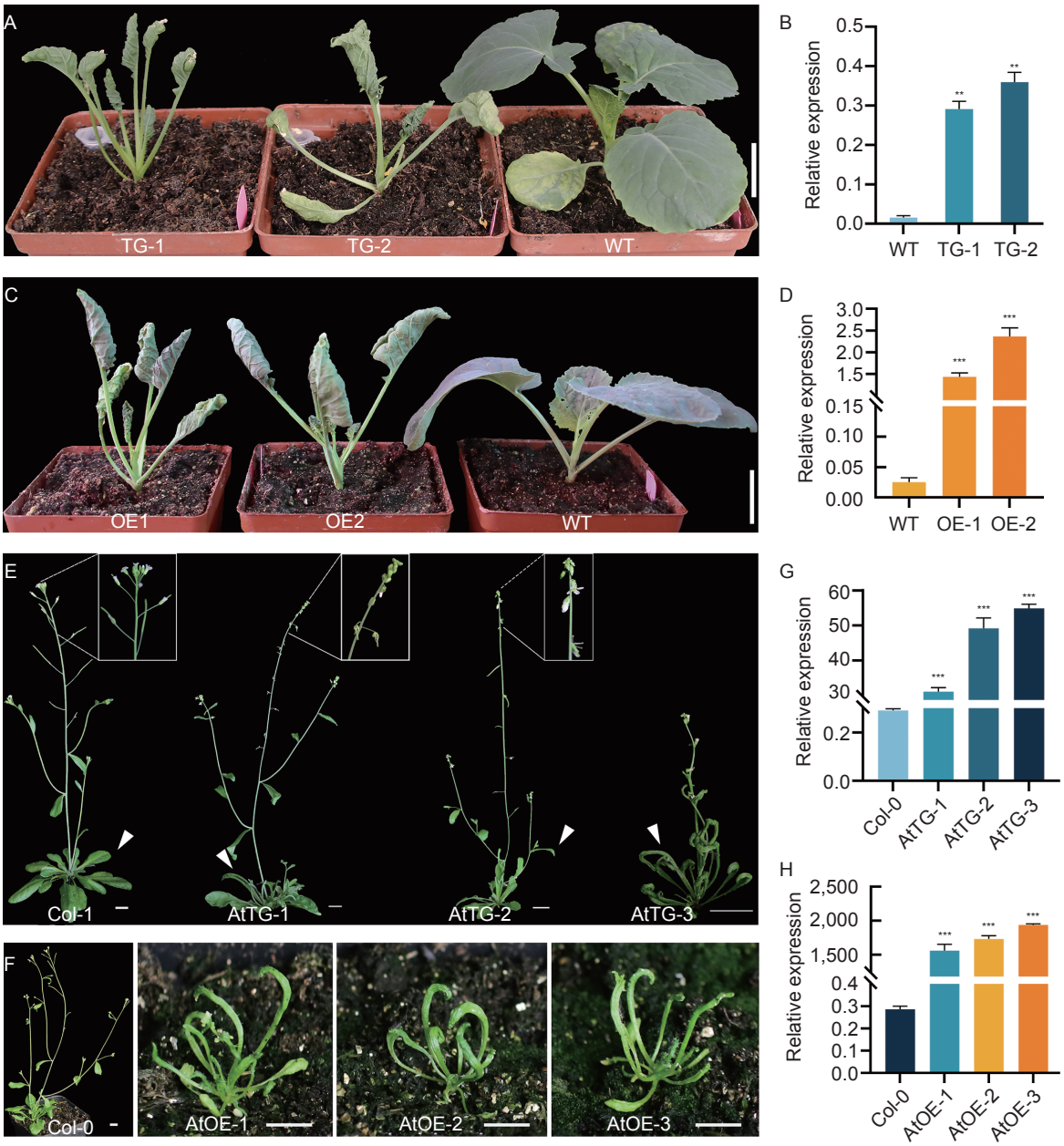


Fig. 4 Complementation and overexpression analyses of *BnaC02.LBD6* in rapeseed and *Arabidopsis*. A, phenotypes of rapeseed complementation lines. The self-promoter of *BnaC02.LBD6*, along with its mutated promoter, was introduced into the wild-type (WT) Westar cultivar. Bar=2.5 cm. B, qRT-PCR analysis of complementation lines in rapeseed revealed a significant upregulation of *BnaC02.LBD6* expression. C, phenotypes of rapeseed overexpression lines. Bar=2.5 cm. D, qRT-PCR analysis of rapeseed overexpression lines showed markedly increased transcript levels of *BnaC02.LBD6*. E, phenotypes of *Arabidopsis* complementation lines. Bar=1 cm. F, phenotypes of *Arabidopsis* overexpression lines. Bar=1 cm. G, qRT-PCR analysis of *Arabidopsis* complementation lines indicated that the severity of phenotypic alterations correlated with the expression level of *BnaC02.LBD6*. H, qRT-PCR analysis of *Arabidopsis* overexpression lines similarly demonstrated a correlation between phenotypic severity and *BnaC02.LBD6* transcript abundance. At, *Arabidopsis*; TG, transgenic line; OE, overexpression line. Bars in B, D, G, and H mean SD (n=3). Statistical significance was determined by Student's t-test: **, P<0.01; ***, P<0.001.

downregulated (Fig. 6-A). Validation of 17 DEGs by qRT-PCR confirmed their expression trends, consistent with RNA-seq data (Appendix M). GO enrichment analysis revealed significant overrepresentation of terms including "response to hormone", "secondary metabolite biosynthetic process", "auxin metabolic process", and "auxin biosynthetic process" (Fig. 6-B). KEGG pathway analysis highlighted enrichment in "auxin biosynthesis", "tryptophan metabolism", "zeatin biosynthesis", "phenylpropanoid biosynthesis", "phenylalanine metabolism", and "cutin, suberine, and wax biosynthesis" (Fig. 6-C). These findings suggest that *BnaC02.LBD6* modulates leaf development by influencing hormone signaling and secondary metabolite pathways.

Analysis of hormone-related DEGs revealed that most were associated with auxin signaling, including members of the YUCCA, AUXIN RESISTANT (AXR), PIN-FORMED

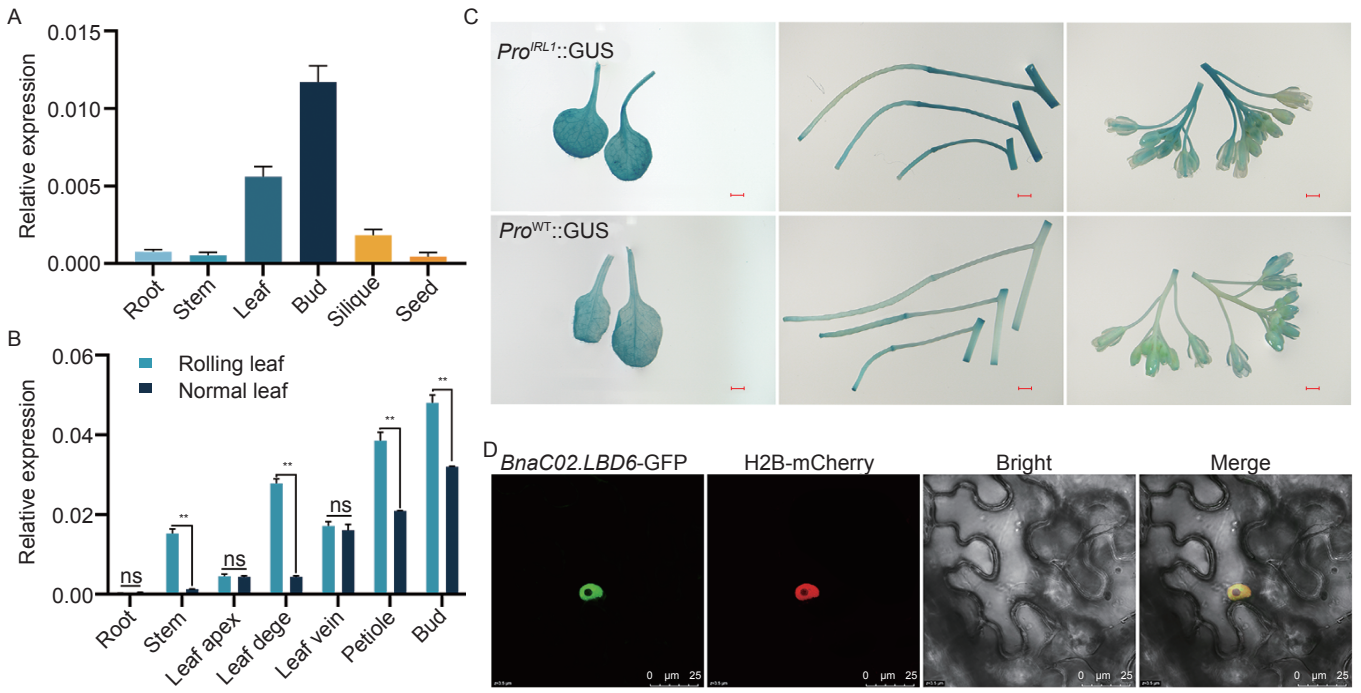


Fig. 5 Expression pattern analysis of *BnaC02.LBD6*. A, *BnaC02.LBD6* was expressed in various tissues, with particularly high expression levels in leaves and buds. B, *BnaC02.LBD6* exhibited differential expression between rolling and normal leaves. Bars in A and B mean SD (n=3). Statistical significance was determined by Student's t-test: **, P<0.01; ns, not significant. C, histochemical β-glucuronidase (GUS) staining. First-row transgenic lines were driven by the mutated promoter; second-row transgenic lines were controlled by the normal promoter. GUS signals driven by the mutated promoter were markedly enhanced Bar=1 mm. D, subcellular localization. *BnaC02.LBD6* colocalized with the nuclear marker H2B-mCherry, indicating nuclear localization.

(PIN), and AUXIN RESPONSE FACTOR (ARF) families, as well as early auxin-responsive genes such as INDOLE-3-ACETIC ACID INDUCIBLE PROTEINs (IAAs), SMALL AUXIN-UPREGULATED RNAs (SAURs), and Gretchen Hagen3 (GH3) genes (Fig. 6-D; Appendix N). Differential expression of these genes likely disrupts auxin biosynthesis, transport, and perception in the *IRL1* mutant, thereby impairing normal leaf development. Additionally, ethylene signaling components, including ETHYLENE-INSENSITIVE (EIN) and ETHYLENE RESPONSE FACTOR (ERF) genes, showed significant expression changes (Fig. 6-C). CYTOKININ OXIDASE/DEHYDROGENASE (CKX) genes were upregulated, and ARABIDOPSIS RESPONSE REGULATOR (ARR) transcripts were differentially expressed (Fig. 6-D; Appendix N), suggesting perturbations in cytokinin homeostasis and signal transduction, which may contribute to abnormal cell division and morphological defects.

4. Discussion

4.1. High expression of *BnaC02.LBD6* leads to disordered development of leaf adaxial–abaxial polarity

Map-based cloning and transgenic complementation assays confirmed that a single nucleotide substitution in the *BnaC02.LBD6* promoter underlies the leaf curling phenotype observed in the *IRL1* mutant. Expression analysis revealed significantly elevated levels of *BnaC02.LBD6* in the mutant (Fig. 5-B and C), and overexpression lines recapitulated the *IRL1* leaf morphology (Fig. 4-B and D). These findings indicate that the promoter mutation causes constitutive overexpression of *BnaC02.LBD6*, thereby driving the phenotypic variation in *IRL1*. *BnaC02.LBD6* is homologous to *Arabidopsis* AS2, which forms a complex with AS1 to regulate adaxial identity during leaf development (Xu *et al.* 2003).

The KANADI (KAN) family plays a critical role in establishing abaxial cell fate, with three members known to contribute to this process (Kerstetter *et al.* 2001; Eshed *et al.* 2004). KAN1 represses the expression of AS2 by directly binding to its promoter, thus maintaining balanced leaf polarity (Wu *et al.* 2008; Chen *et al.* 2013; Machida *et al.* 2015; Burian *et al.* 2022). Sequence alignment revealed that the single nucleotide substitution in the *IRL1* mutant occurs within the KAN1-binding site of the *BnaC02.LBD6* promoter. Yeast one-hybrid (Y1H) assays demonstrated that KAN1 fails to bind the mutated promoter (Appendix O-a and b), confirming that loss of repression leads to *BnaC02.LBD6* overexpression. Furthermore, the AS1/AS2 complex promotes adaxial development by activating HD-ZIP III genes and repressing YABBY family members (McConnell *et al.* 1998; Husbands *et al.* 2015). qRT-PCR analysis showed upregulation of HD-ZIP III genes *REVOLUTA* and *PHABULOSA*, and downregulation of *YABBY* genes *YAB2* and *YAB5* in the *IRL1* mutant (Appendix O-c and d), suggesting that *BnaC02.LBD6* functions through an AS2-like regulatory pathway. Collectively, these data demonstrate that a single promoter mutation disrupts KAN1-mediated repression, resulting in overexpression of *BnaC02.LBD6* and subsequent misregulation of genes governing leaf adaxial–abaxial polarity.

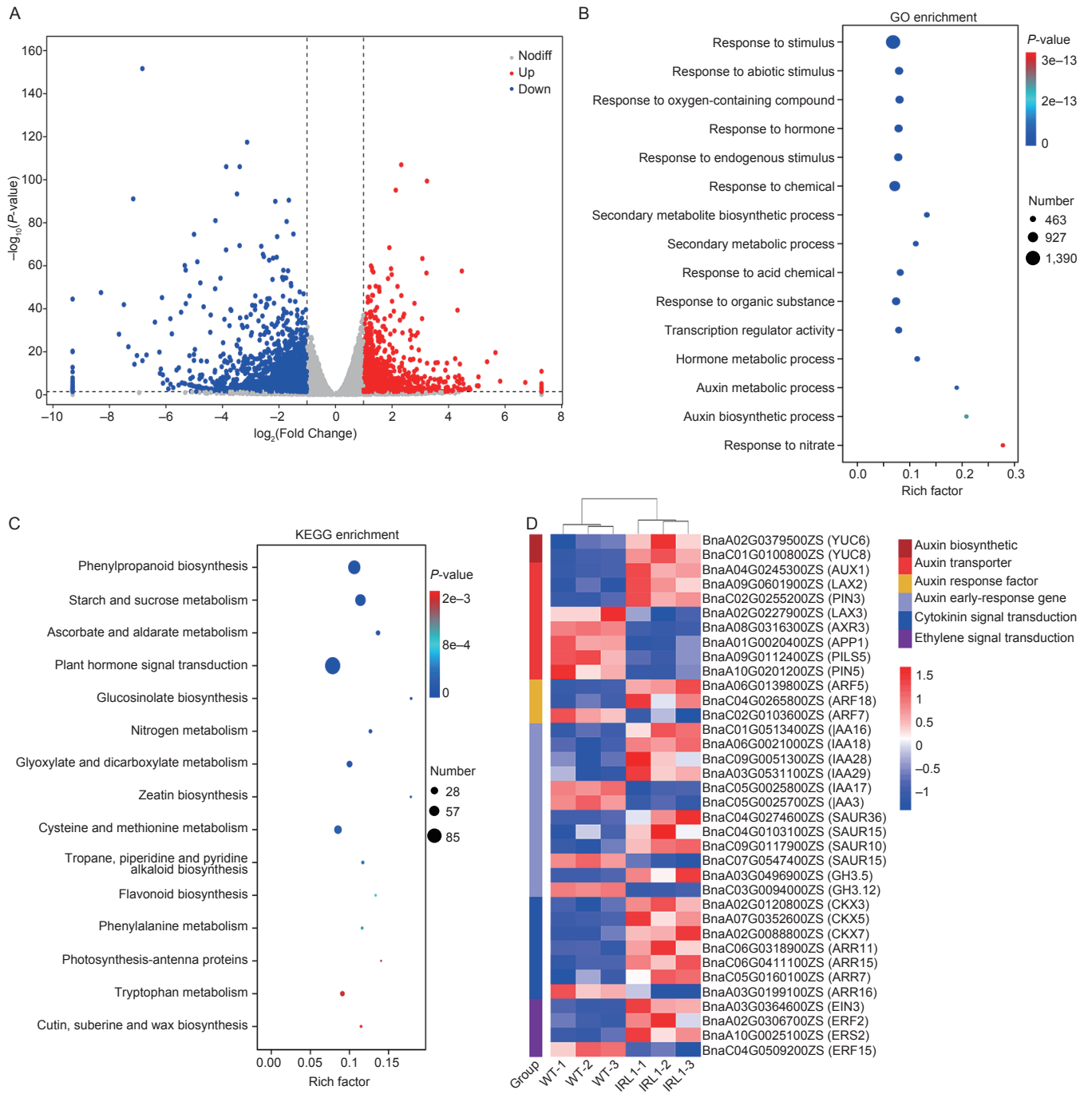


Fig. 6 Transcriptome analysis of transgenic lines and wild-type (WT) Westar. A, volcano plot of differentially expressed genes (DEGs), showing 2,762 upregulated and 1,671 downregulated genes. B, Gene Ontology (GO) enrichment analysis based on DEGs; the top 15 most significantly enriched terms are displayed. C, Kyoto Encyclopedia of Genes and Genomes (KEGG) pathway enrichment analysis based on DEGs; the top 15 most prominent terms are presented. D, heatmap illustrating the expression levels of genes associated with plant hormone signaling pathways.

4.2. *BnaC02.LBD6* may regulate leaf development by affecting secondary metabolites and hormone signalling pathways

Secondary metabolites such as cutin and wax are essential for proper leaf morphogenesis. *OsCFL1* and *AtCFL1*, homologous genes that interact with HDG1, regulate downstream targets BDG and FDH to influence cuticle formation. Mutations in these genes impair cuticle development, leading to rolled leaf phenotypes (Wu *et al.* 2011). Similarly, functional loss of the cuticular wax gene *ZmSRL5* disrupts bulliform cell development and results in semi-rolled leaves (Pan *et al.* 2020). Overexpression of SHINE activates wax biosynthesis, alters cuticle properties, and induces leaf curling (Aharoni *et al.* 2004). In this study, transcriptome profiling revealed significant enrichment of DEGs in pathways including “phenylpropanoid biosynthesis”,

"phenylalanine metabolism", and "cutin, suberine, and wax biosynthesis" (Fig. 6-C). This suggests aberrant synthesis of cuticular components such as wax and suberin in the *IRL1* mutant, implicating *BnaC02.LBD6* in the regulation of secondary metabolic processes during leaf development.

Auxin plays a central role in regulating SHOOT APICAL MERISTEM (SAM) patterning and organ initiation during early leaf development (Su *et al.* 2011; Guenot *et al.* 2012; Qi *et al.* 2014). The *YUCCA* gene, expressed at leaf margins, is required for normal lamina expansion; quadruple mutants (*yuc1 yuc2 yuc4 yuc6*) exhibit narrow leaves lacking typical margin features (Wang *et al.* 2011). *PIN-FORMED1 (PIN1)*, an auxin efflux carrier, modulates leaf polarity by influencing the spatial expression of adaxial–abaxial determinants (Izhaki and Bowman 2007). Additionally, LsKN1 regulates cytokinin and gibberellin homeostasis, and its mutations alter leaf shape in lettuce (Jia *et al.* 2022). In maize, mutations in the cytokinin receptor ZmHK1 enhance cytokinin signaling, altering leaf growth and cellular architecture (Muszynski *et al.* 2020). Transcriptomic analysis in this study revealed dysregulation of auxin biosynthesis and signal transduction pathways (Fig. 6-D). Key components — including YUCCAs, AUX1, PINs, ARFs, and early auxin-responsive genes such as Aux/IAA, SAUR, and GH3 — were abnormally expressed, indicating defects in auxin synthesis, transport, and perception. Moreover, DEGs were enriched in the "zeatin biosynthesis" pathway (Fig. 6-C), and *CYTOKININ OXIDASE/DEHYDROGENASES* were upregulated in the *IRL1* mutant (Appendix N), suggesting disrupted cytokinin homeostasis and signaling. These findings support the conclusion that *BnaC02.LBD6* influences leaf development through modulation of both secondary metabolism and hormonal signaling networks.

4.3. *BnaC02.LBD6* has pleiotropic effects on rapeseed growth and development

Map-based cloning and genetic complementation confirmed *BnaC02.LBD6* as the causal gene underlying the *IRL1* mutant phenotype. A single nucleotide substitution in the promoter abolished KAN1 binding, leading to elevated expression of *BnaC02.LBD6* (Fig. 4). The *IRL1* mutant exhibited curled leaves, and paraffin sectioning revealed disorganized mesophyll cell layers (Fig. 2). Given its homology to *Arabidopsis* AS2, and supported by Y1H and qRT-PCR data, *BnaC02.LBD6* likely regulates leaf polarity via a conserved mechanism (Appendix O). Beyond leaf morphology, the *IRL1* mutant displayed drooping flowers and siliques (Fig. 1-D), a trait validated by complementation assays (Fig. 4-E). In *Arabidopsis*, the KNOX gene *BREVIPEDICELLUS* (*BP*) controls inflorescence architecture, and BP mutants show drooping siliques (Douglas *et al.* 2002; Venglat *et al.* 2002; Li *et al.* 2012; Zhao *et al.* 2015). The AS1/AS2 complex directly regulates BP and KNAT2 expression in leaves (Guo *et al.* 2008; Li *et al.* 2012), linking leaf polarity regulators to reproductive development. Here, expression analysis showed peak LBD6 transcript levels in buds (Fig. 5-A). Notably, BP knockout in rapeseed produces a drooping silique phenotype resembling *IRL1* (Fan *et al.* 2021), suggesting conservation of an LBD6-KNOX regulatory module in inflorescence development. Additionally, the *IRL1* mutant exhibited reduced plant height and fewer effective branches (Fig. 1-C), consistent with transcriptome evidence of disrupted auxin and cytokinin signaling (Fig. 6-D), both of which are critical for overall plant architecture. Thus, *BnaC02.LBD6* exerts pleiotropic effects, influencing leaf shape, inflorescence orientation, plant stature, and branching patterns.

4.4. *BnaC02.LBD6* has potential application value in improving rapeseed plant architecture

Rapeseed plant architecture is defined by leaf arrangement, branching pattern, silique orientation, and plant height. While breeding efforts have traditionally focused on mature-stage traits, vegetative stage architecture has been underemphasized. Current varieties often display fully expanded, horizontally oriented leaves, causing strong interplant shading and limiting light use efficiency and suitability for high-density planting. In contrast, genotypes with compact, upright leaf structures achieve higher population biomass due to improved light penetration and utilization efficiency (Kuai *et al.* 2022). Studies in rice and maize demonstrate that compact architectures enhance yield under dense planting (Sakamoto *et al.* 2006; Tian *et al.* 2019; Li *et al.* 2025), supporting the feasibility of optimizing rapeseed yield through architectural modification. Although branch number contributes to per-plant yield, excessive or late-developing branches can delay seed maturation and compromise harvest quality in high-density systems (Zheng *et al.* 2022). Moreover, widespread use of heterosis has led to tall cultivars in China, typically exceeding 180 cm in height, increasing susceptibility to lodging and impeding mechanization and simplified cultivation. Semi-dwarf types are advantageous for enhancing lodging resistance and enabling efficient mechanical harvesting (Zheng *et al.* 2022; Wang X D *et al.* 2023).

This study demonstrates that LBD6 coordinately regulates multiple agronomic traits in rapeseed, including leaf curvature, plant height, silique posture, and branch number. Hybrid F_1 plants exhibited persistent leaf curling throughout development, which enhances tolerance to dense planting by improving canopy ventilation and light distribution (Appendix A). These hybrids also showed significantly reduced plant height and drooping siliques, with unchanged thousand-seed weight. However, a reduction of one to two effective branches resulted in approximately 14% lower per-plant yield, while the homozygous *IRL1* mutant, with 4–6 fewer branches, suffered a ~40% yield decline (Appendix B). Despite the yield penalty in homozygotes, these architectural traits align well with requirements for intensive, mechanized production systems. Haplotype analysis revealed that the causal SNP in the *BnaC02.LBD6* promoter is unique to the *IRL1* mutant and absent from natural germplasm (Appendix G-a). Based on this variant, a cleaved amplified polymorphic sequence (CAPS) marker was developed to identify alleles with similar functional effects (Appendix P), facilitating marker-assisted

selection in breeding programs.

Previous studies indicate that fine-tuning the expression of dose-sensitive genes offers a viable strategy for crop improvement (Park *et al*. 2014; Je *et al*. 2016; Zhang *et al*. 2017; Hu *et al*. 2019). For example, IPA1 in rice increases panicle number but reduces tillering, limiting its utility; however, CRISPR/Cas9-mediated editing of its regulatory region generated a favorable allele, IPA1-Pro10, which increased yield by 15.9% (Jiao *et al*. 2010; Song *et al*. 2022). These examples underscore the potential of promoter engineering to generate beneficial allelic variants. In this study, the severity of phenotypic changes correlated positively with *BnaC02.LBD6* expression levels (Fig. 4), and yield reductions were more pronounced in homozygous mutants (40%) than in heterozygotes (14%) (Appendix B), indicating a dose-dependent effect on yield. This suggests that weak or partial loss-of-function alleles, achievable through targeted promoter editing, could optimize plant architecture without severe yield penalties. Therefore, *BnaC02.LBD6* represents a promising target for molecular breeding aimed at improving rapeseed plant architecture for modern agricultural systems.

5. Conclusion

This study identified a dominant rapeseed mutant exhibiting rolled leaves. Cytological analysis revealed abnormal mesophyll cell development. Map-based cloning and transgenic validation established *BnaC02.LBD6* as the causal gene. A single nucleotide substitution in its promoter leads to elevated gene expression in the mutant. Transcriptome profiling indicated misregulation of genes involved in secondary metabolism and leaf polarity determination. These findings provide novel insights and valuable germplasm resources for engineering improved rapeseed plant architecture.

Acknowledgements

This work was funded by the National Key Research and Development Program of China (2021YFF1000100) and the Fundamental Research Funds for the Central Universities, China (2662023PY004).

Declaration of competing interest

The authors declare that they have no conflict of interest.

Declaration of generative AI and AI-assisted technologies in the writing process

The authors declare that they did not use AI in the preparation and writing of this manuscript.

Data availability

All relevant data can be found within the manuscript and its supporting materials. The original datasets of RNA-seq have been deposited in the National Center for Biotechnology Information database (accession ID: PRJNA1014567).

Appendices associated with this paper are available at https://doi.org/10.1016/j.jia.2024.06.009

References

Aharoni A, Dixit S, Jetter R, Thoenes E, van Arkel G, Pereira A. 2004. The SHINE clade of AP2 domain transcription factors activates wax biosynthesis, alters cuticle properties, and confers drought tolerance when overexpressed in *Arabidopsis*. *The Plant Cell*, **16**, 2463–2480.

Bowman J L. 2000. The YABBY gene family and abaxial cell fate. *Current Opinion in Plant Biology*, **3**, 17–22.

Burian A, Paszkiewicz G, Nguyen K T, Meda S, Raczyńska-Szajgin M, Timmermans M C P. 2022. Specification of leaf dorsiventrality *via* a prepatterned binary readout of a uniform auxin input. *Nature Plants*, **8**, 269–280.

Caggiano M P, Yu X, Bhatia N, Larsson A, Ram H, Ohno C K, Sappl P, Meyerowitz E M, Jönsson H, Heisler M G. 2017. Cell type boundaries organize plant development. *Elife*, **12**, e27421.

Canales C, Grigg S, Tsiantis M. 2005. The formation and patterning of leaves: Recent advances. *Planta*, **221**, 752–756.

Chen S, Zhou Y, Chen Y, Gu J. 2018. fastp: An ultra-fast all-in-one FASTQ preprocessor. *Bioinformatics*, **34**, i884–i890.

Chen X, Wang H, Li J, Huang H, Xu L. 2013. Quantitative control of ASYMMETRIC LEAVES2 expression is critical for leaf axial patterning in *Arabidopsis*. *Journal of Experimental Botany*, **64**, 4895–4905.

Chitwood D H, Guo M, Nogueira F T, Timmermans M C. 2007. Establishing leaf polarity: The role of small RNAs and positional signals in the shoot apex. *Development*, **134**, 813–823.

Clough S J, Bent A F. 1998. Floral dip: A simplified method for Agrobacterium-mediated transformation of *Arabidopsis thaliana*. *Plant Journal*, **16**, 735–743.

Dkhar J, Pareek A. 2014. What determines a leaf's shape? *Evodevo*, **5**, 47.

Dong J, Huang H. 2018. Auxin polar transport flanking incipient primordium initiates leaf adaxial–abaxial polarity patterning. *Journal of Integrative Plant Biology*, **60**, 455–464.

Douglas S J, Chuck G, Dengler R E, Pelecanda L, Riggs C D. 2002. KNAT1 and ERECTA regulate inflorescence architecture in *Arabidopsis*. *The Plant Cell*, **14**, 547–558.

Du F, Guan C, Jiao Y. 2018. Molecular mechanisms of leaf morphogenesis. *Molecular Plant*, **11**, 1117–1134.

Dun X, Zhou Z, Xia S, Wen J, Yi B, Shen J, Ma C, Tu J, Fu T. 2011. BnaC.Tic40, a plastid inner membrane translocon originating from *Brassica oleracea*, is essential for tapetal function and microspore development in *Brassica napus*. *The Plant Journal*, **68**, 532–545.

Emery J F, Floyd S K, Alvarez J, Eshed Y, Hawker N P, Izhaki A, Baum S F, Bowman J L. 2003. Radial patterning of *Arabidopsis* shoots by class III HD-ZIP and KANADI genes. *Current Biology*, **13**, 1768–1774.

Eshed Y, Baum S F, Perea J V, Bowman J L. 2001. Establishment of polarity in lateral organs of plants. *Current Biology*, **11**, 1251–1260.

Eshed Y, Izhaki A, Baum S F, Floyd S K, Bowman J L. 2004. Asymmetric leaf development and blade expansion in *Arabidopsis* are mediated by KANADI and YABBY activities. *Development*, **131**, 2997–3006.

Fan S, Zhang L, Tang M, Cai Y, Liu J, Liu H, Liu J, Terzaghi W, Wang H, Hua W, Zheng M. 2021. CRISPR/Cas9-targeted mutagenesis of the *BnaA03.BP* gene confers semi-dwarf and compact architecture to rapeseed (*Brassica napus* L.). *Plant Biotechnology Journal*, **19**, 2383–2385.

Fang J, Guo T, Xie Z, Chun Y, Zhao J, Peng L, Zafar S A, Yuan S, Xiao L, Li X. 2021. The URL1-ROC5-TPL2 transcriptional repressor complex represses the *ACL1* gene to modulate leaf rolling in rice. *Plant Physiology*, **185**, 1722–1744.

Garcia D, Collier S A, Byrne M E, Martienssen R A. 2006. Specification of leaf polarity in *Arabidopsis via* the *trans*-acting siRNA pathway. *Current Biology*, **16**, 933–938.

Govaerts Y M, Jacquemoud S, Verstraete M M, Ustin S L. 1996. Three-dimensional radiation transfer modeling in a dicotyledon leaf. *Applied Optics*, **35**, 6585–6598.

Guan C, Wu B, Yu T, Wang Q, Krogan N T, Liu X, Jiao Y. 2017. Spatial auxin signalling controls leaf flattening in *Arabidopsis*. *Current Biology*, **27**, 2940–2950.

Guenot B, Bayer E, Kierzkowski D, Smith R S, Mandel T, Žádníková P, Benková E, Kuhlemeier C. 2012. Pin1-independent leaf initiation in *Arabidopsis*. *Plant Physiology*, **59**, 1501–1510.

Guo M, Thomas J, Collins G, Timmermans M C. 2008. Direct repression

of KNOX loci by the ASYMMETRIC LEAVES1 complex of *Arabidopsis*. *The Plant Cell*, **20**, 48–58.
Howe E S, Clemente T E, Bass H W. 2012. Maize histone H2B-mCherry: A new fluorescent chromatin marker for somatic and meiotic chromosome research. *DNA and Cell Biology*, **31**, 925–938.
Hu Y, Li S, Xing Y. 2019. Lessons from natural variations: Artificially induced heading date variations for improvement of regional adaptation in rice. *Theoretical and Applied Genetics*, **132**, 383–394.
Husbands A Y, Benkovics A H, Nogueira F T, Lodha M, Timmermans M C. 2015. The ASYMMETRIC LEAVES complex employs multiple modes of regulation to affect adaxial–abaxial patterning and leaf complexity. *The Plant Cell*, **27**, 3321–3335.
Itoh J, Hibara K, Sato Y, Nagato Y. 2008. Developmental role and auxin responsiveness of Class III homeodomain leucine zipper gene family members in rice. *Plant Physiology*, **147**, 1960–1975.
Izhaki A, Bowman J L. 2007. KANADI and class III HD-Zip gene families regulate embryo patterning and modulate auxin flow during embryogenesis in *Arabidopsis*. *The Plant Cell*, **19**, 495–508.
Je B I, Gruel J, Lee Y K, Bommert P, Arevalo E D, Eveland A L, Wu Q, Goldshmidt A, Meeley R, Bartlett M, Komatsu M, Sakai H, Jönsson H, Jackson D. 2016. Signaling from maize organ primordia *via* FASCIATED EAR3 regulates stem cell proliferation and yield traits. *Nature Genetics*, **48**, 785–791.
Jia Y, Yu P, Shao W, An G, Chen J, Yu C, Kuang H. 2022. Up-regulation of LsKN1 promotes cytokinin and suppresses gibberellin biosynthesis to generate wavy leaves in lettuce. *Journal of Experimental Botany*, **73**, 6615–6629.
Jiao Y, Wang Y, Xue D, Wang J, Yan M, Liu G, Dong G, Zeng D, Lu Z, Zhu X, Qian Q, Li J. 2010. Regulation of OsSPL14 by OsmiR156 defines ideal plant architecture in rice. *Nature Genetics*, **42**, 541–544.
Kelley D R, Arreola A, Gallagher T L, Gasser C S. 2012. ETTIN (ARF3) physically interacts with KANADI proteins to form a functional complex essential for integument development and polarity determination in *Arabidopsis*. *Development*, **139**, 1105–1109.
Kerstetter R A, Bollman K, Taylor R A, Bomblies K, Poethig R S. 2001. KANADI regulates organ polarity in *Arabidopsis*. *Nature*, **411**, 706–709.
Kim D, Paggi JM, Park C, Bennett C, Salzberg SL. 2019. Graph-based genome alignment and genotyping with HISAT2 and HISAT-genotype. *Nature Biotechnology*, **37**, 907–915.
Kuai J, Li X Y, Ji J L, Li Z, Xie Y, Wang B, Zhou G S. 2022. Response of leaf carbon metabolism and dry matter accumulation to density and row spacing in two rapeseed (*Brassica napus* L.) genotypes with differing plant architectures. *The Crop Journal*, **10**, 680–691.
Li B, Liu X, Guo Y, Deng L, Qu L, Yan M, Li M, Wang T. 2023. BnaC01.BIN2, a GSK3-like kinase, modulates plant height and yield potential in *Brassica napus*. *Theoretical and Applied Genetics*, **136**, 29.
Li C X, Song Y F, Zhu Y, Cao M N, Han X, Fan J S, Lv Z C, Xu Y, Zhou Y, Zeng X, Zhang L, Dong L, Sun D Q, Wang Z H, Di H. 2025. GWAS analysis reveals candidate genes associated with dense tolerance (ear leaf structure) in maize (*Zea mays* L.). *Journal of Integrative Agriculture*, **24**, 2046–2062.
Li H, Li J, Song J, Zhao B, Guo C, Wang B, Zhang Q, Wang J, King G J, Liu K. 2019. An auxin signalling gene *BnaA3.IAA7* contributes to improved plant architecture and yield heterosis in rapeseed. *New Phytologist*, **222**, 837–851.
Li Y, Pi L, Huang H, Xu L. 2012. ATH1 and KNAT2 proteins act together in regulation of plant inflorescence architecture. *Journal of Experimental Botany*, **63**, 1423–1433.
Li Z, Li B, Shen W H, Huang H, Dong A. 2012. TCP transcription factors interact with AS2 in the repression of class-I KNOX genes in *Arabidopsis thaliana*. *The Plant Journal*, **71**, 99–107.
Liao Y, Smyth GK, Shi W. 2014. featureCounts: an efficient general-purpose program for assigning sequence reads to genomic features. *Bioinformatics*, **30**, 923–930.
Machida C, Nakagawa A, Kojima S, Takahashi H, Machida Y. 2015. The complex of ASYMMETRIC LEAVES (AS) proteins plays a central role in antagonistic interactions of genes for leaf polarity specification in *Arabidopsis*. *Wiley Interdisciplinary Reviews* (Developmental Biology), **4**, 655–671.
Manuela D, Xu M. 2020. Patterning a leaf by establishing polarities. *Frontiers in Plant Science*, **11**, 568730.
McConnell J R, Barton M K. 1998. Leaf polarity and meristem formation in *Arabidopsis*. *Development*, **125**, 2935–2942.
McConnell J R, Emery J, Eshed Y, Bao N, Bowman J, Barton M K. 2001. Role of PHABULOSA and PHAVOLUTA in determining radial patterning in shoots. *Nature*, **411**, 709–713.
Merelo P, Paredes E B, Heisler M G, Wenkel S. 2017. The shady side of leaf development: The role of the REVOLUTA/KANADI1 module in leaf patterning and auxin-mediated growth promotion. *Current Opinion in Plant Biology*, **35**, 111–116.
Merelo P, Ram H, Pia Caggiano M, Ohno C, Ott F, Straub D, Graeff M, Cho S K, Yang S W, Wenkel S, Heisler M G. 2016. Regulation of MIR165/166 by class II and class III homeodomain leucine zipper proteins establishes leaf polarity. *Proceedings of the National Academy of Sciences of the United States of Ameirica*, **113**, 11973–11978.
Moon J, Hake S. 2011. How a leaf gets its shape. *Current Opinion in Plant Biology*, **14**, 24–30.
Muszynski M G, Moss-Taylor L, Chudalayandi S, Cahill J, Del Valle-Echevarria A R, Alvarez-Castro I, Petefish A, Sakakibara H, Krivosheev D M, Lomin S N, Romanov G A, Thamotharan S, Dam T, Li B, Brugière N. 2020. The maize *Hairy Sheath Frayed1* (*Hsf1*) mutation alters leaf patterning through Increased cytokinin signaling. *The Plant Cell*, **32**, 1501–1518.
Pan Z, Liu M, Zhao H, Tan Z, Liang K, Sun Q, Gong D, He H, Zhou W, Qiu F. 2020. ZmSRL5 is involved in drought tolerance by maintaining cuticular wax structure in maize. *Journal of Integrative Plant Biology*, **62**, 895–1909.
Park S J, Jiang K, Tal L, Yichie Y, Gar O, Zamir D, Eshed Y, Lippman Z B. 2014. Optimization of crop productivity in tomato using induced mutations in the florigen pathway. *Nature Genetics*, **46**, 1337–1342.
Pekker I, Alvarez J P, Eshed Y. 2005. Auxin response factors mediate *Arabidopsis* organ asymmetry *via* modulation of KANADI activity. *The Plant Cell*, **17**, 2899–2910.
Prigge M J, Otsuga D, Alonso J M, Ecker J R, Drews G N, Clark S E. 2005. Class III homeodomain-leucine zipper gene family members have overlapping, antagonistic, and distinct roles in *Arabidopsis* development. *The Plant Cell*, **17**, 61–76.
Qi J, Wang Y, Yu T, Cunha A, Wu B, Vernoux T, Meyerowitz E, Jiao Y. 2014. Auxin depletion from leaf primordia contributes to organ patterning. *Proceedings of the National Academy of Sciences of the United States of Ameirica*, **111**, 18769–18774.
Romanova M A, Maksimova A I, Pawlowski K, Voitsekhovskaja O V. 2021. YABBY genes in the development and evolution of land plants. *International Journal of Molecular Sciences*, **22**, 4139.
Rong F, Chen F, Huang L, Zhang J, Zhang C, Hou D, Cheng Z, Weng Y, Chen P, Li Y. 2019. A mutation in class III homeodomain-leucine zipper (HD-ZIP III) transcription factor results in curly leaf (cul) in cucumber (*Cucumis sativus* L.). *Theoretical and Applied Genetics*, **132**, 113–123.
Sakamoto T, Morinaka Y, Ohnishi T, Sunohara H, Fujioka S, Ueguchi-Tanaka M, Mizutani M, Sakata K, Takatsuto S, Yoshida S, Tanaka H, Kitano H, Matsuoka M. 2006. Erect leaves caused by brassinosteroid deficiency increase biomass production and grain yield in rice. *Nature Biotechnology*, **24**, 105–109.
Sarojam R, Sappl P G, Goldshmidt A, Efroni I, Floyd S K, Eshed Y, Bowman J L. 2010. Differentiating *Arabidopsis* shoots from leaves by combined YABBY activities. *The Plant Cell*, **22**, 2113–2130.
Satterlee J W, Scanlon M J. 2019. Coordination of leaf development across developmental axes. *Plants*, **8**, 433.
Siegfried K R, Eshed Y, Baum S F, Otsuga D, Drews G N, Bowman J L. 1999. Members of the YABBY gene family specify abaxial cell fate in *Arabidopsis*. *Development*, **126**, 4117–4128.
Song X, Meng X, Guo H, Cheng Q, Jing Y, Chen M, Liu G, Wang B, Wang Y, Li J, Yu H. 2022. Targeting a gene regulatory element enhances rice grain yield by decoupling panicle number and size. *Nature Biotechnology*, **40**, 1403–1411.
Stahle M I, Kuehlich J, Staron L, von Arnim A G, Golz J F. 2009. YABBYs and the transcriptional corepressors LEUNIG and LEUNIG_HOMOLOG maintain leaf polarity and meristem activity in *Arabidopsis*. *The Plant Cell*, **21**, 3105–3118.
Su Y H, Liu Y B, Zhang X S. 2011. Auxin-cytokinin interaction regulates meristem development. *Molecular Plant*, **4**, 616–625.
Sun J, Cui X, Teng S, Kunnong Z, Wang Y, Chen Z, Sun X, Wu J, Ai P, Quick W P, Lu T, Zhang Z. 2020. HD-ZIP IV gene *Roc8* regulates the size of bulliform cells and lignin content in rice. *Plant Biotechnology*

Journal, **18**, 2559–2572.
Tang S, Liu D X, Lu S, Yu L, Li Y, Lin S, Li L, Du Z, Liu X, Li X, Ma W, Yang Q Y, Guo L. 2020. Development and screening of EMS mutants with altered seed oil content or fatty acid composition in *Brassica napus*. *The Plant Journal*, **104**, 1410–1422.
Tang S, Zhao H, Lu S, Yu L, Zhang G, Zhang Y, Yang Q Y, Zhou Y, Wang X, Ma W, Xie W, Guo L. 2021. Genome- and transcriptome-wide association studies provide insights into the genetic basis of natural variation of seed oil content in *Brassica napus*. *Molecular Plant*, **14**, 470–487.
Tatematsu K, Toyokura K, Miyashima S, Nakajima K, Okada K. 2015. A molecular mechanism that confines the activity pattern of miR165 in *Arabidopsis* leaf primordia. *The Plant Journal*, **82**, 596–608.
Tian J, Wang C, Xia J, Wu L, Xu G, Wu W, Li D, Qin W, Han X, Chen Q, Jin W, Tian F. 2019. Teosinte ligule allele narrows plant architecture and enhances high-density maize yields. *Science*, **365**, 658–664.
Venglat S P, Dumonceaux T, Rozwadowski K, Parnell L, Babic V, Keller W, Martienssen R, Selvaraj G, Datla R. 2022. The homeobox gene BREVIPEDICELLUS is a key regulator of inflorescence architecture in *Arabidopsis*. *Proceedings of the National Academy of Sciences of the United States of Ameirica*, **99**, 4730–4735.
Wang H, Kong F, Zhou C. 2021. From genes to networks: The genetic control of leaf development. *Journal of Integrative Plant Biology*, **63**, 1181–1196.
Wang J, Xu J, Wang L, Zhou M, Nian J, Chen M, Lu X, Liu X, Wang Z, Cen J, Liu Y, Zhang Z, Zeng D, Hu J, Zhu L, Dong G, Ren D, Gao Z, Shen L, Zhang Q, *et al.* 2023. SEMI-ROLLED LEAF 10 stabilizes catalase isozyme B to regulate leaf morphology and thermotolerance in rice (*Oryza sativa* L.). *Plant Biotechnology Journal*, **21**, 819–838.
Wang W, Xu B, Wang H, Li J, Huang H, Xu L. 2011. YUCCA genes are expressed in response to leaf adaxial–abaxial juxtaposition and are required for leaf margin development. *Plant Physiology*, **157**, 1805–1819.
Wang X D, Cai Y, Pang C K, Zhao X Z, Shi R, Liu H F, Chen F, Zhang W, Fu S X, Hu M L, Hua W, Zheng M, Zhang J F. 2023. BnaSD.C3 is a novel major quantitative trait locus affecting semi-dwarf architecture in *Brassica napus*. *Journal of Integrative Agriculture*, **22**, 2981–2992.
Wu D, Liang Z, Yan T, Xu Y, Xuan L, Tang J, Zhou G, Lohwasser U, Hua S, Wang H, Chen X, Wang Q, Zhu L, Maodzeka A, Hussain N, Li Z, Li X, Shamsi I H, Jilani G, Wu L, *et al.* 2019. Whole-genome resequencing of a worldwide collection of rapeseed accessions reveals the genetic basis of ecotype divergence. *Molecular Plant*, **12**, 30–43.
Wu G, Lin W C, Huang T, Poethig R S, Springer P S, Kerstetter R A. 2008. KANADI1 regulates adaxial–abaxial polarity in Arabidopsis by directly repressing the transcription of ASYMMETRIC LEAVES2. *Proceedings of the National Academy of Sciences of the United States of Ameirica*, **105**, 16392–16397.
Wu R, Li S, He S, Wassmann F, Yu C, Qin G, Schreiber L, Qu L J, Gu H. 2011. CFL1, a WW domain protein, regulates cuticle development by modulating the function of HDG1, a class IV homeodomain transcription factor, in rice and *Arabidopsis*. *The Plant Cell*, **23**, 3392–3411.
Xu L, Xu Y, Dong A, Sun Y, Pi L, Xu Y, Huang H. 2003. Novel as1 and as2 defects in leaf adaxial-abaxial polarity reveal the requirement for ASYMMETRIC LEAVES1 and 2 and ERECTA functions in specifying leaf adaxial identity. *Development*, **130**, 4097–4107.
Xu P, Ali A, Han B, Wu X. 2018. Current advances in molecular basis and mechanisms regulating leaf morphology in rice. *Frontiers in Plant Science*, **23**, 1528.
Yu X Q, Xie W, Liu H, Liu W, Zeng D L, Qian Q, Ren D Y. 2022. Characterization and fine mapping of a semi-rolled leaf mutant *srl3* in rice. *Journal of Integrative Agriculture*, **21**, 3103–3113.
Zhang L, Yu H, Ma B, Liu G, Wang J, Wang J, Gao R, Li J, Liu J, Xu J, Zhang Y, Li Q, Huang X, Xu J, Li J, Qian Q, Han B, He Z, Li J. 2017. A natural tandem array alleviates epigenetic repression of IPA1 and leads to superior yielding rice. *Nature Communications*, **8**, 14789.
Zhao M, Yang S, Chen C Y, Li C, Shan W, Lu W, Cui Y, Liu X, Wu K. 2015. *Arabidopsis* BREVIPEDICELLUS interacts with the SWI2/SNF2 chromatin remodeling ATPase BRAHMA to regulate KNAT2 and KNAT6 expression in control of inflorescence architecture. *PLoS Genetics*, **11**, 1005125.
Zheng M, Terzaghi W, Wang H, Hua W. 2022. Integrated strategies for increasing rapeseed yield. *Trends In Plant Science*, **27**, 742–745.
Zhu Z, Wang J, Li C, Li L, Mao X, Hu G, Wang J, Chang J, Jing R. 2022. A transcription factor TaMYB5 modulates leaf rolling in wheat. *Frontiers in Plant Science*, **13**, 897623.

Executive Editor-in-Chief Xueyong Zhang
Managing Editor Ning Wang